

# Detecting Dental Landmarks from Intraoral 3D Scans: the 3DTeethLand challenge

Achraf Ben-Hamadou<sup>a</sup>, Nour Neifar<sup>a</sup>, Ahmed Rekik<sup>a</sup>, Oussama Smaoui<sup>b</sup>, Firas Bouzguenda<sup>b</sup>, Sergi Pujades<sup>c</sup>, Niels van Nistelrooij<sup>d</sup>, Shankeeth Vinayahalingam<sup>d</sup>, Kaibo Shi<sup>e</sup>, Hairong Jin<sup>e</sup>, Youyi Zheng<sup>e</sup>, Tibor Kubík<sup>f,g</sup>, Oldřich Kodým<sup>f</sup>, Petr Šilling<sup>f,g</sup>, Kateřina Trávníčková<sup>f</sup>, Tomáš Mojžiš<sup>f</sup>, Jan Matula<sup>f</sup>, Jeffry Hartanto<sup>h</sup>, Xiaoying Zhu<sup>i</sup>, Kim-Ngan Nguyen<sup>j</sup>, Tudor Dascalu<sup>k</sup>, Huikai Wu<sup>l</sup>, Weijie Liu<sup>m</sup>, Shaojie Zhuang<sup>m</sup>, Guangshun Wei<sup>m</sup>, Yuanfeng Zhou<sup>m</sup>

<sup>a</sup>*Centre de Recherche en Numérique de Sfax, Laboratory of Signals, Systems, Artificial Intelligence and Networks, Technopôle de Sfax, 3021 Sfax, Tunisia*

<sup>b</sup>*Udini, 37 BD Aristide Briand, 13100 Aix-En-Provence, France*

<sup>c</sup>*Inria, Univ. Grenoble Alpes, CNRS, Grenoble INP, LJK, France*

<sup>d</sup>*Department of Oral and Maxillofacial Surgery Radboud University Medical Center Geert Grooteplein Zuid 10 6525 GA Nijmegen Netherlands*

<sup>e</sup>*State Key Lab of CAD&CG, Zhejiang University, Hangzhou, 310058, China*

<sup>f</sup>*TESCAN 3DIM, s.r.o., Brno, Czech Republic*

<sup>g</sup>*Department of Computer Graphics and Multimedia, Brno University of Technology, Brno, Czech Republic*

<sup>h</sup>*National Dental Centre Singapore*

<sup>i</sup>*Guangxi Colleges and Universities Key Laboratory of Intelligent Software, Wuzhou University*

<sup>j</sup>*National University of Singapore*

<sup>k</sup>*Department of Computer Science, University of Copenhagen*

<sup>l</sup>*Hangzhou ChohoTech Inc*

<sup>m</sup>*School of Software, Shandong University, China*

---

## Abstract

Teeth landmark detection is a critical task in modern clinical orthodontics. Their precise identification enables advanced diagnostics, facilitates personalized treatment strategies, and supports more effective monitoring of treatment progress in clinical dentistry. However, several significant challenges may arise due to the intricate geometry of individual teeth and the substantial variations observed across different individuals. To address these complexities, the development of advanced techniques, especially through the application of deep learning, is essential for the precise and reliable detection of 3D tooth landmarks. In this context, the 3DTeethLand challenge was held in collaboration with the International Conference on Medical Image Computing and Computer-Assisted Intervention (MICCAI) in 2024, calling for algorithms focused on teeth landmark detection from intraoral 3D scans. This challenge introduced the first publicly available dataset for 3D teeth landmark detection, offering a valuable resource to assess the state-of-the-art methods in this task and encourage the community to provide methodological contributions towards the resolution of their problem with significant clinical implications.

*Keywords:* 3D intraoral scans, dental landmark detection, 3D landmark detection

---

## 1. Introduction

Digital tools like computer-aided design (CAD) have become essential in contemporary dentistry, enabling highly precise treatment planning. Advanced intraoral scanners (IOSs) are particularly pivotal in orthodontic CAD systems, as they produce accurate 3D digital models of the teeth [1]. These digital models serve as the foundation for various orthodontic applications, such as teeth alignment and treatment simulation [2, 3]. One of the most essential tools for such applications is the detection of key dental landmarks. These landmarks, including features such as cusps and mesial-distal locations, serve as fundamental reference points for diagnosing dental conditions, designing personalized treatment plans, and evaluating treatment progress [4]. Accurate identification of these landmarks plays an essential role in advancing orthodontic procedures, enabling precise alignments, improving occlusal relationships, and enhancing the overall efficiency and outcomes of dental care. However, several significant challenges may arise due to the intricate geometry of individual teeth, including variations in shape, size, orientation, as well as the presence of pathological teeth [5]. Considerable inter-individual differences, such as variations in dental arch forms, tooth alignment, and occlusal relationships, further complicate these challenges.

To address this, developing advanced techniques has become a central focus of research, particularly by leveraging the potential of deep learning for the accurate detection of 3D tooth landmarks. However, the limited availability of publicly accessible data presents a significant challenge, as the success of such approaches, as well as their fair comparison, depends heavily on the availability of well-annotated datasets.

In this context, the 3DTeethLand challenge <sup>1</sup> was organized in collaboration with the International Conference on Medical Image Computing and Computer-Assisted Intervention (MICCAI) in 2024, alongside two other challenges: ToothFairy [6] and STS [7]. The 3DTeethLand challenge specifically called for algorithms aimed at detecting teeth landmarks from intraoral 3D scans. To support this effort, we also present the first publicly available database prepared for the challenge, with the goal of advancing research in 3D tooth landmark detection. The result announcement was held during the satellite event dedicated to the challenge at MICCAI 2024.

## 2. Related work to teeth landmark detection

Unlike the segmentation task, which is widely studied [8, 9], the number of studies on tooth landmark detection (*i.e.*, localization) is still limited. Previous studies can be grouped into two main categories: traditional methods [4, 10] and deep learning-based approaches [11, 12, 13, 14, 15]. Some of these methods adopt a generalized framework involving both tooth segmentation and landmark detection [11, 12, 14].

---

*Email address:* `achraf.benhamadou@crns.rnrt.tn` (Achraf Ben-Hamadou)

<sup>1</sup><https://crns-smartvision.github.io/teeth3ds/#3DTeethLandSec>

The work presented in [4, 10] relies on traditional approaches for landmark detection. In [4], the proposed method follows consecutive steps including approximating the dental surface orientation, identifying local maxima to locate landmarks, segmenting teeth using surface features, removing non-tooth parts via rule-based filtering and jaw-line fitting, and labeling teeth and detecting landmarks for each tooth. Meanwhile, the approach in [10] combines deep learning for tooth segmentation and a weighted mesh points method for landmark detection. The landmark detection approach draws inspiration from [4], incorporating unit vector orientation, unit vector sign determination, and landmark point identification. These traditional methods rely on handcrafted features such as curvature, local maxima, and surface orientation, which may not generalize well across diverse dental models or handle variations such as missing teeth or deformities.

Wei *et al.* [12] proposed a deep learning method for landmark and axis detection from a 3D tooth model. In this framework, the landmarks and axes are encoded as dense fields defined on the surface of a tooth model. This approach incorporates multi-scale feature extraction and feature enhancement modules to capture both local and global features. While this approach is effective, its reliance on k-means clustering introduces several limitations, particularly regarding computational efficiency and flexibility, especially when dealing with varying numbers of landmarks or different tooth model characteristics.

Wu *et al.* [11] presented the TS-MDL framework, a two-stage method for joint tooth labeling and landmark identification. The first stage employs an end-to-end iMeshSegNet, a variant of MeshSegNet [16, 17], to label each tooth on the downsampled scan. In the second stage, TS-MDL uses the segmentation results to identify the region of interest (ROI) for each tooth on the original mesh, then employs a lightweight version of PointNet, named PointNet-Reg, to predict the corresponding landmark heatmaps that encode landmark locations. The advantage of this method lies in its efficiency, as the heatmap predictions are directly used to identify landmarks, eliminating the need for additional post-processing steps. However, a significant limitation is its reliance on a predefined number of landmarks, which makes the method unsuitable for cases where the number and type of landmarks vary across different teeth.

Lang *et al.* [14] proposed the DLLNet, an end-to-end deep learning framework for automatically localizing 68 landmarks on high-resolution 3D dental models. It follows a coarse-to-fine two-stage approach. The first stage involves tooth segmentation using the MeshSegNet on a down-sampled mesh, while the second stage refines landmark locations by applying their proposed DLLNet to mesh patches around the initial coarse localization. This model extracts multi-scale local contextual features through collaborative task-driven paths, one focused on landmark localization and the other on area segmentation. Additionally, the framework incorporates curvature features, alongside traditional vertex coordinates, normal vectors, and cell centroids, providing a more detailed structural representation of landmark areas. To further enhance detection accuracy, the model incorporates an attention mechanism, enabling it to focus on the most relevant areas during landmark localization. However, this model has two key limitations. First, it cannot automatically detect missing teeth or adapt to patients with jaw deformities, which presents a significant challenge. Second, its reliance on pre-segmented tooth partitions for landmark localization makes it susceptible to

segmentation errors, which can negatively impact the model’s robustness and precision.

Recently, the authors introduced the deep learning framework DentalPointNet [13], designed to automatically locate 68 landmarks on high-resolution dental surface models represented as point clouds. This framework follows a two-stage coarse-to-fine approach. The first stage focuses on the coarse localization of each landmark using a curvature-constrained region proposal network (RPN). In the second stage, DLLNet is applied to small groups of points around the coarse localization results to refine the landmark locations. By considering the landmark localization task as an object detection problem, this method aims to minimize the risk of false negatives, even in challenging scenarios, such as in the case of missing teeth.

Tibor *et al.* [15] introduced a tooth landmark detection method leveraging a multi-view approach that transforms the task into the 2D domain. In the approach, a CNN-based network is used to detect landmarks by regressing heatmaps from multiple viewpoints. To map the detected landmarks back into 3D space, the authors proposed using the RANSAC consensus. Additionally, to address the problem of estimation of landmarks on missing teeth, the authors introduced a post-processing step which is based on uncertainty analysis. This analysis combines the Maximum Heatmap Activation Confidence and the Multi-view Confidence that quantify the heatmap regression uncertainty and the uncertainty of the multi-view approach, respectively.

### 3. Challenge setup

This section provides an overview of our database, including details on data annotation and recorded information.

#### 3.1. Database

Most state-of-the-art research in this domain relies on a limited number of scans, none of which are publicly accessible [15]. In contrast, we offer a significantly larger dataset that is publicly available <sup>2</sup>, which has the potential to accelerate progress in this field. The database [18] was initially created for the 3DTeethSeg 2022 MICCAI challenge [8], to advance research in the analysis of intraoral 3D scans, including tasks such as teeth identification, segmentation, and labeling. The dataset was collected following the European General Data Protection Regulation (GDPR), in collaboration with orthodontists and dental surgeons with over five years of professional experience from partner dental clinics, primarily based in France and Belgium. All patient information has been anonymized to ensure complete confidentiality. The dataset is released under the CC BY-NC-ND license, allowing sharing with attribution while restricting commercial use and derivative works.

For each patient in the dataset, two 3D scans were obtained, one for the upper jaw and one for the lower jaw.

For the 3DTeethLand Challenge, we provided landmark annotations on a dataset comprising 340 intraoral scans (IOS). The dataset is split into two groups:

---

<sup>2</sup><https://crns-smartvision.github.io/teeth3ds/>

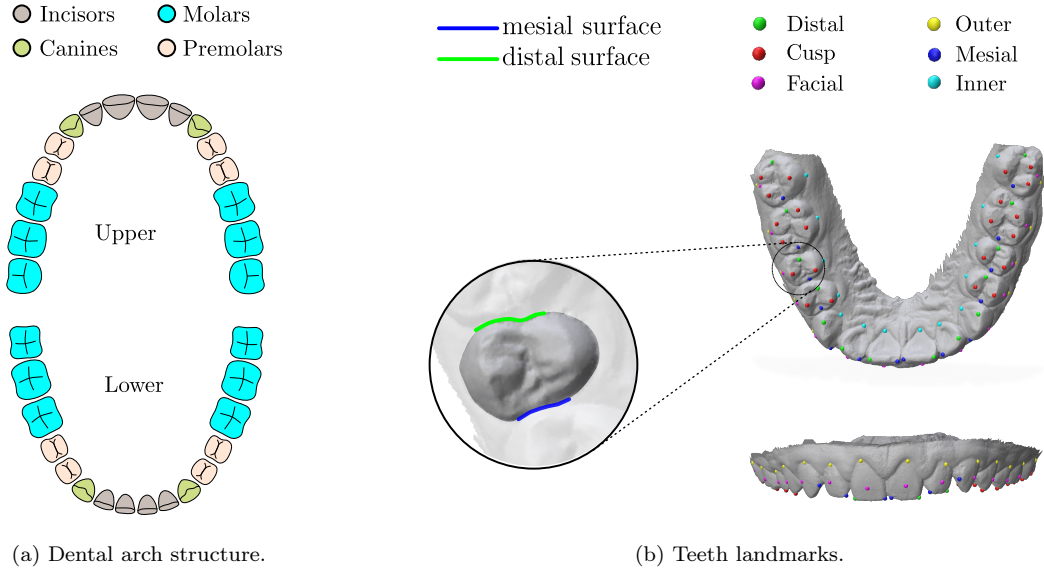


Figure 1: Overview of tooth structure and anatomical landmarks. (a) Illustration of the human dental arches showing the distribution of incisors, canines, premolars, and molars in the upper and lower jaws. (b) 3D intraoral scans annotated with key dental landmarks, including distal, mesial, facial, cusp, outer, and inner points used for geometric analysis.

- The first group includes 240 scans from the Teeth3DS dataset, including segmentation and labeling annotations, and serving as the training set for the challenge.
- The second group consists of 100 unannotated scans that form the hidden private test set.

### 3.2. Data acquisition:

The scans were acquired using state-of-the-art intraoral 3D scanners—specifically the Primescan (Dentsply), TRIOS 3 (3Shape), and iTero Element 2 Plus. These devices are widely adopted in clinical practice and are known to produce high-quality 3D models, with accuracies ranging from 10 to 90  $\mu\text{m}$  and point resolutions between 30 and 80 pts/ $\text{mm}^2$ .

No specific acquisition protocol was imposed other than requiring complete coverage of both the upper and lower jaws. Acquisitions were performed by orthodontists or dental surgeons with more than five years of professional experience, while the challenge’s clinical evaluators have over ten years of expertise in orthodontics, dental surgery, and endodontics.

The dataset includes patients undergoing either orthodontic treatment (50%) or prosthetic treatment (50%). Ethical approval for data collection and use was granted by the Local Ethics Committee of the Digital Research Center, University of Sfax (Tunisia) on 28 October 2020 under approval number PV-CS-28/10/2020. In addition, the study was validated by DELSOL Avocats (Paris, France), a law firm specializing in GDPR compliance.

### 3.3. Data annotation

Teeth have a complex anatomical structure, consisting of various surfaces and features. They are categorized into four main types based on their shape and function, as shown in Figure 1a: incisors, canines, premolars, and molars. Landmarks on these teeth serve as key reference points, facilitating the accurate measurement of tooth orientations, spacing, and occlusion. To ensure precise analysis of tooth positioning and alignment, specific dental landmarks are identified on each tooth, providing a standardized approach for consistent and reproducible assessments. The annotation process was carried out iteratively by professional annotators using a custom tool developed by our clinical partner, Udini. Annotators were instructed to identify and label every tooth landmark class on each tooth within the intraoral 3D scans. Following this, a final validation phase was carried out by experienced dentists. Each scan was initially annotated by a single annotator, after which all annotations were systematically reviewed and verified by the three clinical evaluators of the challenge. This multi-step procedure ensures both the accuracy and reliability of the landmark annotations.

Figure 1b depicts an overview of the landmarks annotation. This annotation includes:

*Mesial and Distal points.* The mesial surface of a tooth refers to the side of the tooth that faces the center of the mouth. While, the distal surface is the opposite of the mesial, meaning it faces away from the midline of the mouth (See Figure 1b). The mesial and distal points represented in red and green, respectively, in Figure 1b are located on the mesial and distal surfaces. These points are crucial for assessing the alignment and positioning of the tooth within the dental arch, helping to evaluate its relationship to adjacent teeth.

*Cusp points.* The cusp refers to the pointed or rounded elevation on the chewing surface of a tooth. The cusp point, highlighted in blue in Figure 1b, is situated at the highest point of the cusp, playing a key role in understanding the occlusion relationship between the upper and lower teeth during biting and chewing. The number of cusp points varies depending on the type of tooth. For instance, premolars typically have two cusps, whereas molars typically present three to five cusps (See Figure 1b).

*Inner and outer points.* The inner points, represented in yellow in Figure 1b, and outer points, depicted in cyan, are defined at the boundary where the tooth meets the gingiva, serving as key anatomical reference points. The inner point is positioned on the lingual or palatal side of the tooth, closer to the tongue or the palate, while the outer point is located on the buccal side, facing the cheeks or lips. These landmarks are essential for analyzing the spatial pose and orientation of the tooth within the dental arch.

*Facial axis point.* The facial axis point, represented in magenta, is located at the center of the facial surface of each tooth, which is the side visible from the front of the mouth. This point is significant for understanding the tooth’s angulation and inclination and is crucial for accurate alignment analysis and orthodontic planning.

The distribution of the test landmarks across six categories is as follows:

```

{
  "version": "1.1",
  "description": "landmarks",
  "key": "01A6GW4A_upper.obj",
  "objects": [
    {"key": "uuid_0", "class": "Mesial", "coord": [6.422, -20.096, -84.301]},
    ...
    {"key": "uuid_14", "class": "Distal", "coord": [3.796, -19.872, -83.586]},
    ...
    {"key": "uuid_28", "class": "Inner", "coord": [-5.895, -17.951, -84.251]},
    ...
    {"key": "uuid_42", "class": "Outer", "coord": [-26.155, 11.975, -89.822]},
    ...
    {"key": "uuid_66", "class": "Cusp", "coord": [-18.206, -0.849, -89.995]},
    ...
    {"key": "uuid_80", "class": "FacialPoint", "coord": [-26.176, 22.662, -91.674]}
  ]
}

```

Figure 2: Example of the file structure of landmarks annotation.

- Cusp: 1374 points
- Mesial: 1366 points
- Inner: 1351 points
- Facial: 1358 points
- Distal: 2343 points
- Outer: 1350 points

### 3.4. Data records

Landmark annotations for each intraoral scan in the dataset are delivered in JavaScript Object Notation (JSON) format. An example of the file structure is shown in Figure 2. This file provides essential information, including the version of the file format and the unique identifier for the corresponding intraoral scan. It also contains a list of objects representing the landmark points identified on the scan. Each object is described by a unique key that serves as an identifier for the point, its class, and its 3D coordinates.

## 4. Top ranked methods

A total of 49 teams officially participated in the 3DTeethLand challenge, with 115 team members preregistered. During the preliminary phase, 10 teams made their submissions, and 6 teams proceeded to the final phase with their final submissions uploaded to the leaderboard. The participating algorithms are required to detect all visible teeth within each intraoral 3D scan. All the algorithms submitted by participants were run on the Synapse platform<sup>3</sup>. Submission instructions<sup>4</sup> were published on the webpage to guide participants in

<sup>3</sup><https://www.synapse.org/Synapse:syn57400900/wiki/>

<sup>4</sup><https://www.synapse.org/Synapse:syn57400900/wiki/629180>

submitting their Docker files to the evaluation platform. After submitting their Docker files, the teams received an email indicating whether the submission ran successfully, along with a link where they could view the execution logs and the evaluation result on one randomly selected training case. The training algorithms were not limited to the data provided by the challenge. However, participants were asked to provide a description of all datasets used for training to ensure a fair comparison.

Table 1 provides a summary of the top six ranked methods, which will be explored in-depth in the subsequent section for a comprehensive understanding of their approaches. For clarity, a specific color is assigned to each team, which is used consistently in both the tables and the experimental results. These methods can be divided into two main categories. The first category follows the typical setup involving tooth segmentation followed by landmark detection. The second category does not involve tooth segmentation.

Table 1: Summary of the participating methods

Team/Ref. Authors	Approach characteristics
<p>■ Radboud (Niels van Nistelrooij <i>et al.</i>)</p>	<p><b>Tooth instance segmentation:</b> Seed Map generation, Instance identification, Tooth label prediction, Multiclass Segmentation. <b>Tooth landmark detection:</b> High-resolution segmentation, Landmark detection.</p>
<p>■ YY-LAB (Kaibo Shi <i>et al.</i>)</p>	<p><b>3D tooth segmentation:</b> Resolution Reduction, Feature Extraction, TeethGNN Model, Graph-Cut Refinement, Projection and Cropping. <b>Landmark detection:</b> Input Features Extraction, TeethGNN Encoder, Global Features Processing, Decoding Process, Fixed Landmarks Prediction, and Cusp Landmarks Prediction.</p>
<p>■ YN-LAB (Zhu Xiaoying <i>et al.</i>)</p>	<p><b>Tooth segmentation</b> Data preprocessing, multi-step segmentation algorithm, Point jittering and Downsampling with FPS, <b>Landmark detection:</b> Coarse and detail landmark detection.</p>
<p>■ IGIP-LAB (Weijie Liu <i>et al.</i>)</p>	<p><b>Landmark detection:</b> Point cloud transformation, Euclidean distance field calculation, PointTransformer V3 for prediction, Post-processing.</p>
<p>■ ChohoTech (Huikai Wu)</p>	<p><b>Landmark detection:</b> Data preprocessing, DGCNN model with two output branches (probability heatmap and offset regression), Post-processing.</p>
<p>■ 3DIMLAND (Tibor Kubik <i>et al.</i>)</p>	<p><b>Landmark detection:</b> Geometry encoding, Distance decoding, and CTD-NMS refinement.</p>

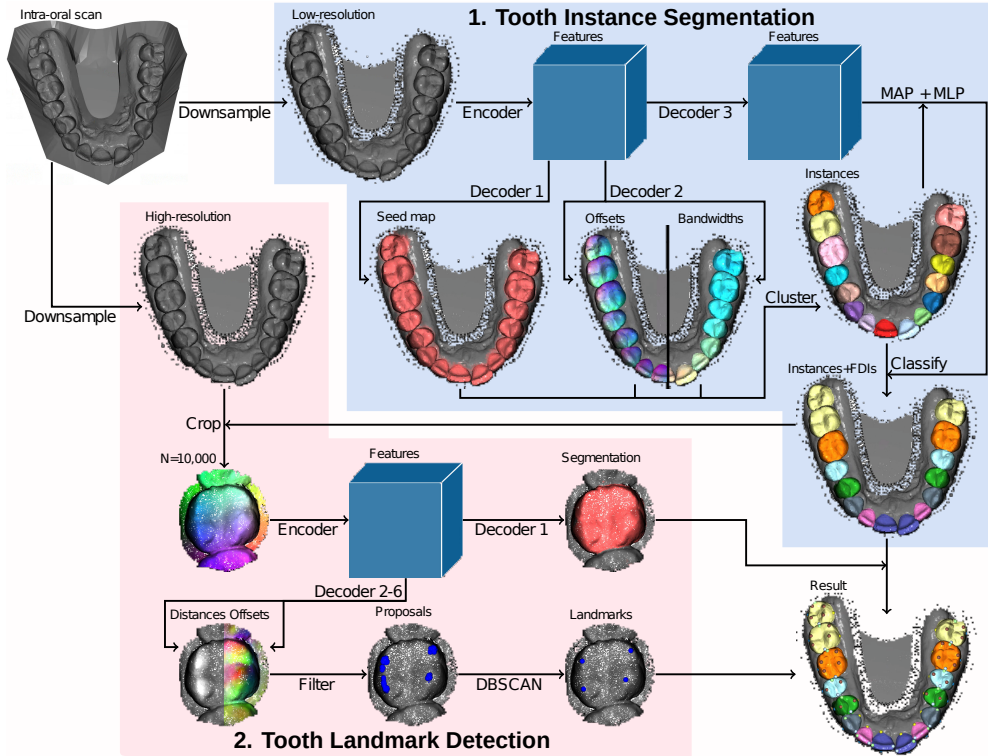


Figure 3: Overview of the proposed method by the Radboud team. The method consists of two stages dedicated to tooth instance segmentation and tooth landmark detection.

#### 4.1. ■ Radboud team (Niels van Nistelrooij *et al.*)

The proposed approach by Niels van Nistelrooij *et al.* is shown in Figure 3. Their method follows a two-stage process. The first stage performs end-to-end tooth instance segmentation and labeling, leveraging a large context specifically optimized for accurate tooth labeling. In the second stage, high-resolution tooth crops are analyzed to refine the tooth segmentation and to independently predict landmarks of each landmark class.

##### 4.1.1. Tooth instance segmentation

In this step, the surface mesh is first transformed into a downsampled point cloud to reduce the number of points for processing. Then, a shared encoder along with three separate decoders are employed. The first decoder generates a seed map for binary semantic segmentation of teeth, with higher seed values indicating points closer to a tooth center. The second decoder estimates offsets from points to their nearest tooth center as well as bandwidths. Tooth instances are identified iteratively, selecting the highest seed value to define a Gaussian distribution representing the tooth’s position and size. Points with a probability above 0.5 based on this Gaussian distribution are clustered to form a tooth instance. This process continues until no high seed values remain. The third decoder extracts features from the encoder for tooth labeling, averaging features of each instance to create an instance embedding by masked average pooling, which is processed by a multi-layer perceptron to

predict tooth labels. Finally, by combining tooth instance segmentation and tooth labeling, a multiclass tooth instance segmentation is obtained.

#### 4.1.2. Tooth landmark detection

The model dedicated to landmark detection processes single-tooth crops and is made up of one shared encoder and six separate decoders. The first decoder generates a high-resolution binary segmentation of the center tooth, enhancing the accuracy of the low-resolution segmentation produced during the tooth instance segmentation stage. Decoders two through six were tasked with detecting specific landmarks: mesial and distal (decoder two), facial (decoder three), inner (decoder four), outer (decoder five), and cusp landmarks (decoder six). By assigning different decoders to distinct landmark classes, the model achieved improved accuracy in positioning each landmark. For example, decoder six identifies the nearest cusp landmark by estimating distances and offsets for each point. Points within a defined distance threshold are adjusted based on their offsets to create landmark proposals. These proposals are then clustered using the weighted DBSCAN algorithm [19], where the weights are inversely related to the predicted distances. A landmark’s final position is determined by calculating the weighted average of the cluster’s landmark proposals. Lastly, mesial and distal landmarks from decoder two are categorized using a rule-based approach, relying on the tooth’s FDI number and the landmarks’ relative position to the tooth center.

#### 4.2. ■ YY-LAB team (Kaibo Shi *et al.*)

Since landmark detection directly from a jaw model is highly challenging, the YY-LAB team proposed 3D tooth segmentation as an initial phase. As shown in Figure 4, the proposed method by Kaibo Shi *et al.* consists of two stages: 3D tooth segmentation and landmark detection.

##### 4.2.1. Tooth Segmentation

To address challenges during network training and inference, the authors proposed reducing the resolution of jaw meshes from over 100,000 facets to approximately 10,000 using mesh decimation algorithm [20]. Features extracted from the facets, comprising centroid coordinates, facet normals, and vectors from each of the three vertices to the centroid, will be the input into the TeethGNN model [21]. This model generates semantic labels, which are further refined using the graph-cut algorithm to improve boundary definition. After, projecting back the refined labels onto the original mesh, the teeth will be cropped into tooth patches from the jaw model according to these segmentation results.

##### 4.2.2. Landmark detection

For landmark detection for individual teeth, the authors were inspired by the Keypoint-DETR [22] and proposed TL-DETR. In this network, two decoder branches are considered: a fixed landmark branch and a cusp landmark branch, as the number of cusp points varies based on the tooth’s shape and type, while other landmarks are fixed on every tooth. Given a single tooth patch, TL-DETR predicts heatmaps for the fixed landmarks and both heatmaps

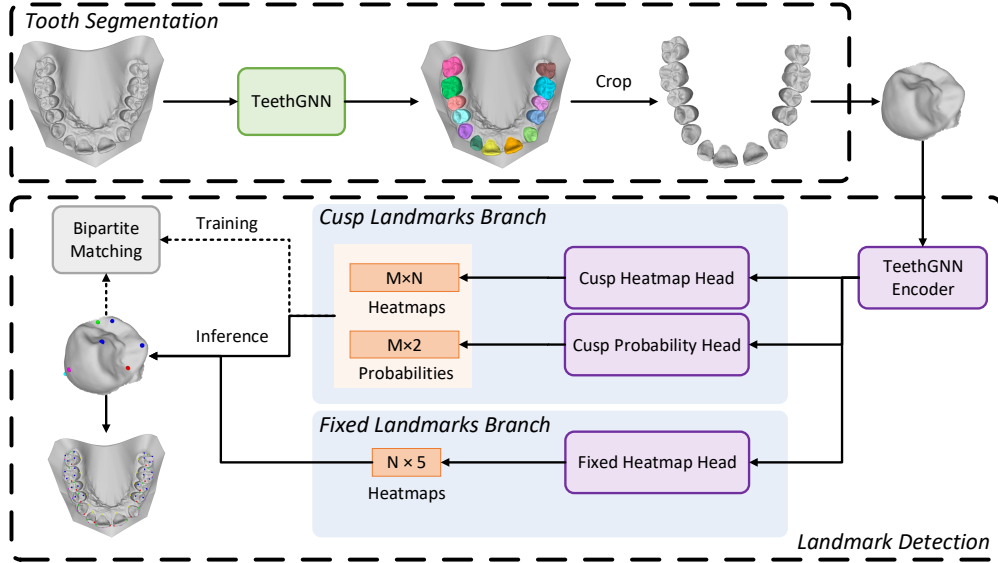


Figure 4: Overview of the proposed method proposed by the YY-LAB team. The presented approach consists of two stages: 3D tooth segmentation and landmark detection.

and probabilities for the potential cusp landmarks. Following a process similar to tooth segmentation, facet features are first extracted and fed into the network. These features are processed by the TeethGNN encoder, which utilizes static EdgeConv layers to capture local geometric information. Fully connected and pooling layers then generate global features, which are combined with the local features and decoded through another EdgeConv layer to produce the final feature representation. The decoding process consists of two branches tailored for fixed and cusp landmarks. For fixed landmarks, the feature representation is passed to a heatmap head comprising an MLP and Conv1d layers, producing heatmaps for the five fixed landmarks. For cusp landmarks, the feature is decoded into a heatmap feature, which is then processed by separate heatmap and probability heads. These heads generate heatmaps representing cusp landmark locations and binary probabilities distinguishing between cusp landmarks and background points. The bipartite matching loss is used to measure the discrepancy between the prediction sets and the ground truth cusp heatmaps, facilitating end-to-end inference.

#### 4.3. ■ YN-LAB team (Zhu Xiaoying et al.)

The proposed method adopts the curriculum learning paradigm [23], where the training process is organized to gradually tackle tasks of growing complexity. It begins with an initial segmentation task targeting larger regions of interest around the ground-truth landmarks, and it progresses to a more detailed segmentation task focusing on smaller regions. The global pipeline of this approach is presented in Figure 5.

##### 4.3.1. Data Pre-processing

In this step, an input 3D jaw model was processed to segment out the tooth region only, which addresses potential data imbalance since the tooth region occupies a small

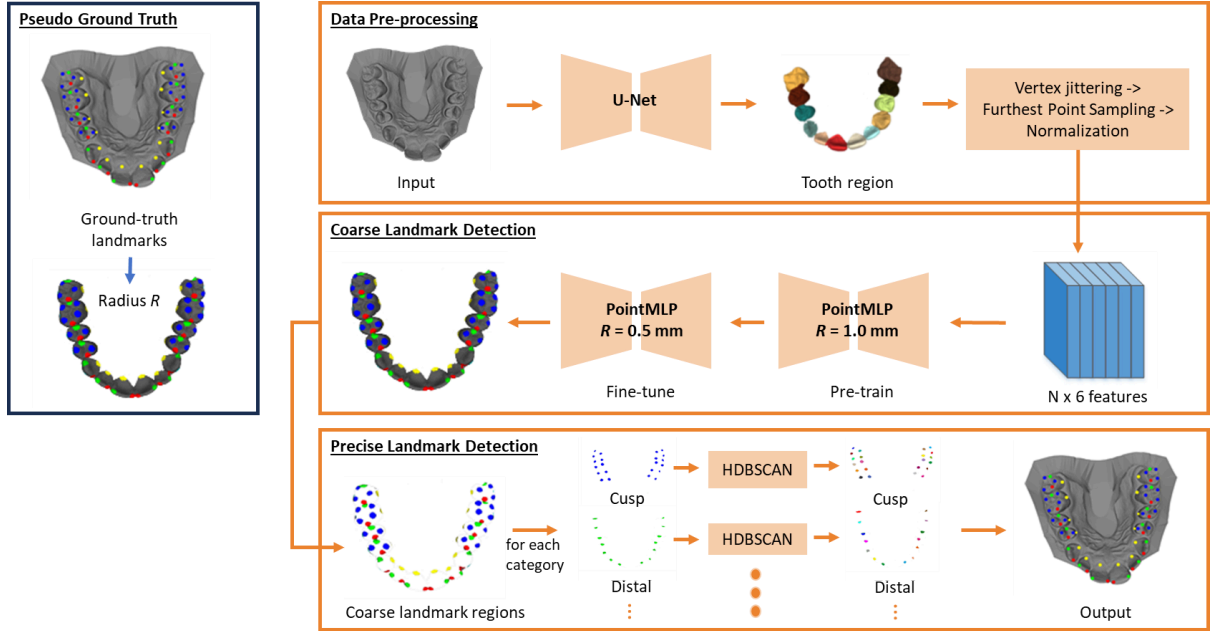


Figure 5: Overview of the proposed method proposed by the YN-LAB team: Tooth segmentation and data augmentation are performed as a preliminary step, followed by coarse landmark detection guided by the pseudo ground truth and precise landmark detection.

region over the entire surface of the jaw model. Moreover, all tooth landmarks are located within the tooth region. This tooth segmentation process was done using the coarse-to-fine segmentation algorithm proposed by the TeethSeg in the 3DTeethSeg’22 challenge [8, 24], which refines the tooth-gingival boundary to achieve accurate tooth segmentation. To reduce model overfitting, the segmented tooth region undergoes several steps of data augmentation. First, vertex jittering was applied by adding Gaussian noise at several levels of intensity to the points in the segmented regions, which potentially covers tooth shape variations. Next, Farthest Point Sampling (FPS) [25] was used to ensure a well-distributed distribution of downsampled points from the segmented tooth region. Lastly, the downsampled points were normalised to be within a unit sphere, and their normal vectors were computed.

#### 4.3.2. Landmark detection

This step is composed of two main phases: coarse landmark detection and precise landmark detection. Coarse landmark detection aims to segment the region around the landmark. It takes  $N$  normalized points, which include both points’ coordinates and normal vectors. Then, it leverages the PointMLP network [26] to effectively capture both the point cloud’s local and global features and perform the segmentation task. The training process is guided by pseudo ground truths, i.e., points within radius  $R$  from each landmark were assigned the landmark’s label. Empirically, the authors found that the network was unable to perform accurate segmentation with small  $R$  directly, potentially due to severe data imbalance. Therefore, they adopted a curriculum learning approach to enhance the segmentation ac-

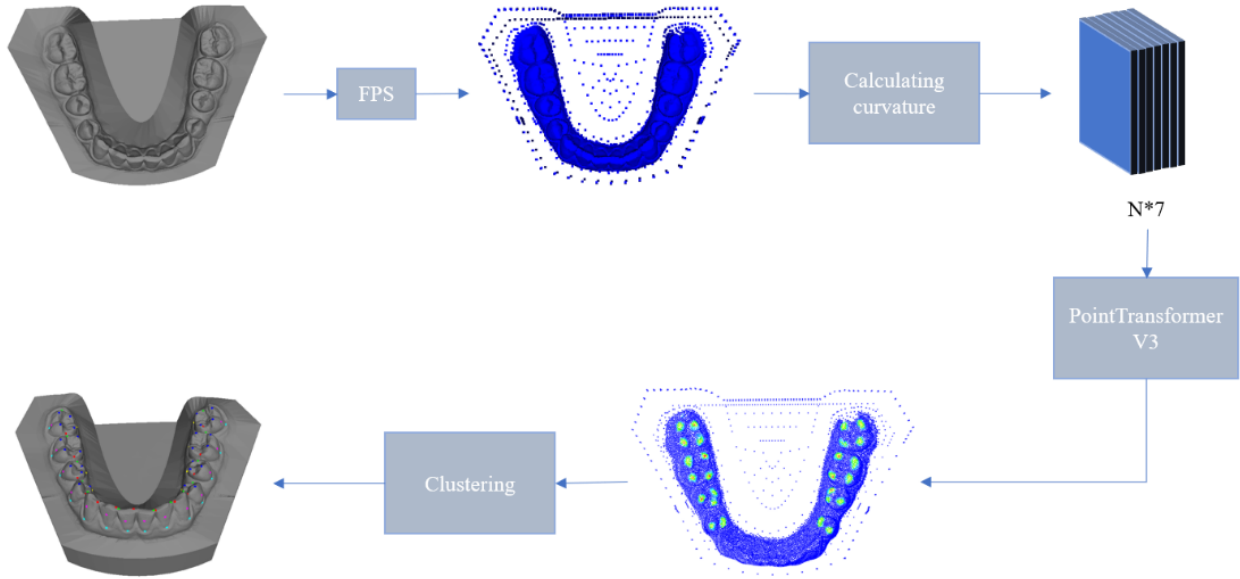


Figure 6: Global pipeline of the proposed approach by the IGIP-LAB team.

curacy. Initially, the network was pre-trained on a pseudo ground truth with a radius  $R$  of 1.0 mm until convergence. Next, the pre-trained network was fine-tuned on pseudo ground truth with a smaller radius  $R$  of 0.5 mm until convergence, which is a more complex task. This curriculum learning-inspired approach gives more accurate segmentation results.

The precise landmark detection stage uses the segmented region from the coarse landmark detection to determine the precise location of each landmark within it. In this step, the HDBSCAN clustering algorithm [27] was employed to group segmented points belonging to a specific landmark’s category based on their points’ density. After the clustering, Gaussian weighted voting is used. This method assigns higher importance to points closer to the cluster center, which serves as the detected tooth landmark.

#### 4.4. ■ IGIP-LAB team (Weijie Liu *et al.*)

The global pipeline of the proposed method by Weijie Liu *et al.*, which does not include a segmentation step, is presented in Figure 6. In their approach, the authors proposed transforming 3D tooth models into point cloud data to enhance the model’s ability to capture complex geometries. Therefore, they started by sampling 16384 points from each model to obtain the corresponding point cloud data, which includes both coordinate and normal information using the FPS. Next, the curvature of each point is calculated using the obtained normal data. In addition, the Euclidean distance field between landmarks and corresponding teeth is calculated. This distance field is then used to guide the network training by translating these distances into confidence levels. With the PointTransformer V3 as the foundational architecture, the network will be used to predict the confidence levels for various landmark categories. The final step is a post-processing step that filters out landmarks with confidence values below 0.7. The remaining landmarks are grouped via density-based clustering, with the highest-confidence landmark in each cluster selected as the final landmark.

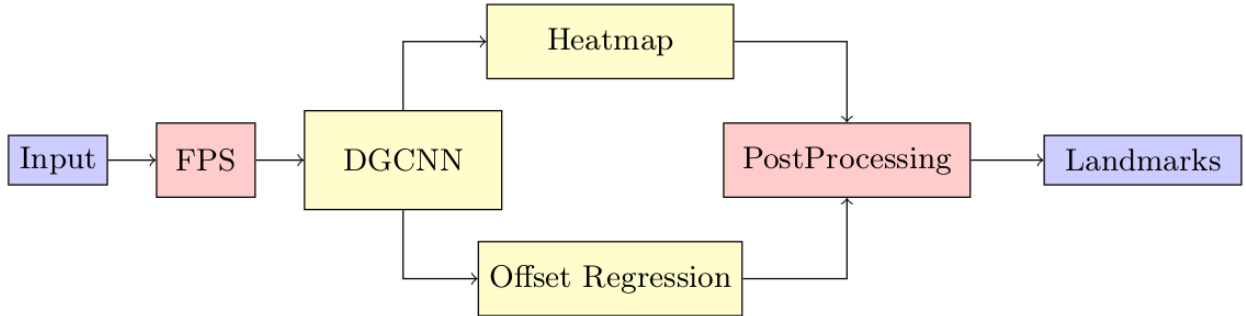


Figure 7: Overview of the proposed method by the ChohoTech team.

#### 4.5. ■ ChohoTech team (Huikai Wu)

The proposed approach by Huikai Wu also does not involve segmentation. An overview of his approach is depicted in Figure 7. This 3D dental landmark detection method involves several key steps, beginning with data preprocessing. First, 3D intraoral scan models are resampled using FPS to generate consistent point clouds, with each patch characterized by its center coordinates, normal vector, and vertices. The following features will serve as input to the proposed network. Its architecture is based on Dynamic Graph Convolutional Networks (DGCNN), which includes two output branches: one for estimating the likelihood of a point being a landmark (probability heatmap) and another for calculating the residual vector from each point to its nearest landmark (offset regression). At each layer, the network performs a K-Nearest Neighbor (KNN) search based only on the input point coordinates, enabling it to capture local geometric relationships. Finally, a post-processing stage is performed that applies confidence thresholding to filter out low-confidence points. In addition, a Non-Maximum Suppression (NMS) is applied to eliminate redundant detections, ensuring precise landmark identification.

#### 4.6. ■ 3DIMLAND team (Tibor Kubík *et al.*)

Figure 8 depicts the global pipeline of the proposed method by Tibor Kubík *et al.*. This method leverages transformer architectures to model a function that predicts landmark positions from an input mesh representing a single 3D dental scan. The framework is composed of three key components: a geometry encoder, a distance decoder, and a graph-based non-minima suppression module. The role of the Geometry Encoder step is to process the dental mesh into a meaningful, latent feature space. Since dental meshes have varying numbers of vertices, this step ensures consistency by randomly selecting a fixed number of points from the original mesh, reducing the complexity caused by varying mesh resolutions. To avoid sampling irrelevant mesh regions, the proposed method ensures that the sampled points are focused primarily on the important parts of the mesh, such as the teeth and gingiva, rather than unnecessary structures. Additionally, it enriches the point cloud by concatenating vertex normal information, providing the model with more geometric context. The Distance Decoder in this framework takes the learned per-point features from the Geometry Encoder and maps them into a 6-channel per-point distance output. This design allows

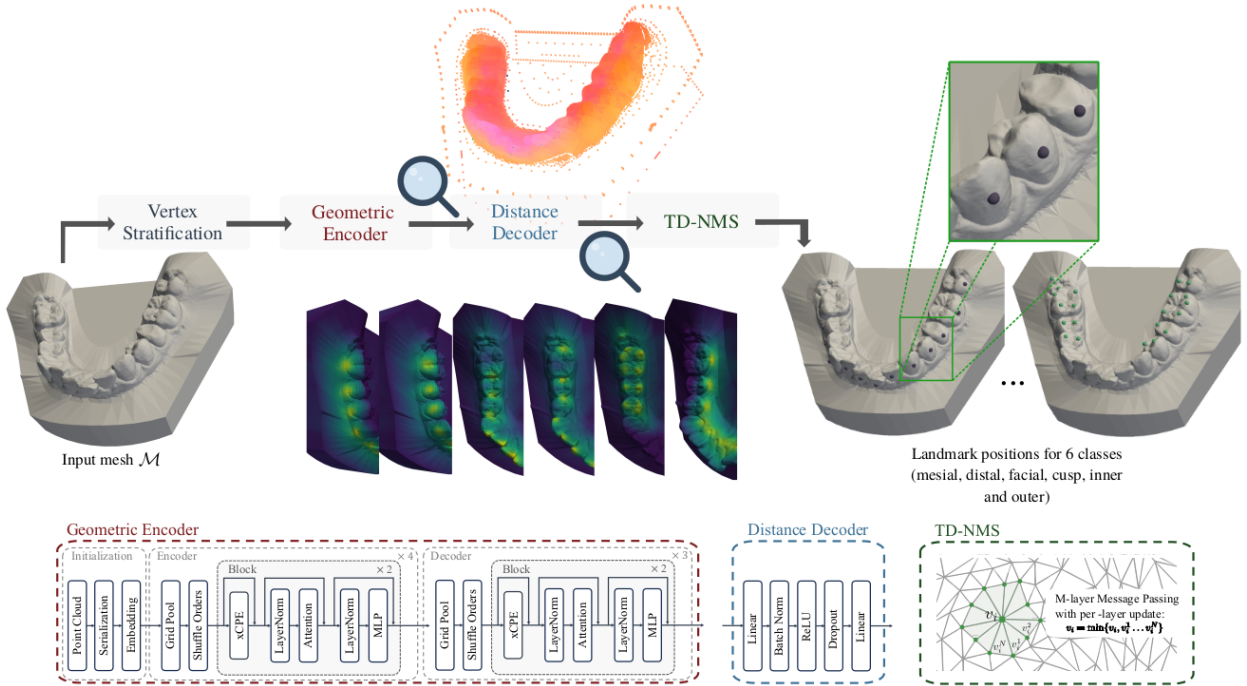


Figure 8: Overview of the method proposed by the 3DIMLAND team.

the framework to detect landmarks in six different categories without needing intra-class label assignment. The Calibrated Topology-Driven Non-Minima Suppression (CTD-NMS) module is employed to refine the landmark extraction process from the distance decoder’s output. While a basic approach might involve extracting the maxima from the thresholded distance maps, it is prone to producing clusters of false positives, particularly when the input geometry provides insufficient information. To address this issue, the authors proposed the CTD-NMS, which uses a graph-convolutional operator to iteratively update each vertex’s value by considering its neighbors in the mesh, ensuring only the most robust landmarks are retained. A vertex is classified as a landmark if its value remains unchanged and its distance is below a predefined threshold, with the parameters calibrated based on model performance and mesh resolution.

## 5. Experimental results

In this section, we detail the employed evaluation metrics, describe the ranking protocol, and present the obtained results.

### 5.1. Evaluation metrics

Within the existing literature, various metrics such as root mean square error (RMSE) [10], mean distance error (MDE) [12], and mean absolute error (MAE) [11], have been commonly used for the assessment of landmark localization, typically assuming a fixed number of landmarks. However, our challenge context differs from this norm as we are dealing with

a detection task involving a variable number of landmarks per tooth. In this context, and in line with [28] and [29], we considered two metrics, the **Mean Average Precision** (mAP) and the **Mean Average Recall** (mAR), as these metrics are more suitable and align more effectively with the nature of this task. To evaluate the accuracy of landmark detection, we categorize the landmarks into four distinct groups according to their clinical relevance, as outlined below:

- Category 1: Mesial/Distal
- Category 2: Cusps
- Category 3: Outer/Inner
- Category 4: Facial

The mAP is computed by aggregating the Average Precision (AP) values across different landmark categories. Each AP is derived from the area under the Precision-Recall curve and evaluated at multiple distance thresholds. As a result, we calculate a distinct mAP value for each landmark category, providing a comprehensive assessment of detection performance across the different landmarks.

Similarly, the **mAR** is calculated by aggregating the Average Recall (AR) for each category, where AR is determined by the area under the Recall-exp(-Distance) curve. As with mAP, the number of mAR values corresponds to the number of landmark categories.

The localization criterion is defined by the Euclidean distance between predicted and reference landmarks. A prediction is considered a valid detection (or "hit") if the Euclidean distance between the predicted and reference landmarks falls below a predefined threshold. Given the varying clinical requirements for landmark localization, multiple thresholds are used to assess the performance of the detection algorithm. These thresholds range from 0 mm to 3 mm, incremented by 0.1 mm, capturing a broad spectrum of practical scenarios.

For the landmark assignment, a greedy strategy is employed, wherein predicted landmarks are ranked based on their predicted class scores. The assignment proceeds by iteratively matching each predicted landmark, starting from the highest score to the nearest reference landmark. It is important to note that each reference landmark can only be assigned to one predicted landmark, ensuring a one-to-one correspondence. This strategy optimizes the matching process while maintaining robustness in the evaluation of detection accuracy.

## 5.2. Ranking protocol

To ensure robust rankings, we employed a point-based ranking method enhanced by bootstrapping. The process begins with the computation of the mAP and mAR metrics for each landmark category. Teams are then pairwise compared for each metric using the Wilcoxon Signed Rank Test. A team is awarded one point for each comparison where it is deemed statistically superior ( $p - value < 0.001$ ), resulting in a "total point count" that reflects the number of comparisons won. Bootstrapping is applied by resampling 10% of the data and repeating the pairwise comparison process on the remaining data, generating a "total point count" for each resampling iteration. This process is repeated 100 times. The final point score for each team is normalized by the total number of comparisons,

calculated as the normalized scores are then aggregated to produce the final ranking, ensuring a statistically robust and fair evaluation of performance.

### 5.3. Obtained results

The performance of each participating team was evaluated based on the proposed ranking protocol, as detailed in the previous section. The results are summarized in Tables 2, 3, and 4, which collectively provide a comprehensive overview of team performance.

Table 2 presents the overall performance metrics, including the Rank Score, mAP, and mAR. The Rank Score reflects a statistically robust ranking that combines both precision and recall metrics. Radboud team (Niels van Nistelrooij *et al.*) achieved the highest Rank Score of 0.9172, with a corresponding mAP of 0.785 and mAR of 0.656, indicating an outstanding balance between precision and recall. On the other hand, the 3DIMLAND team (Tibor Kubík *et al.*) ranked lowest with a Rank Score of 0.0325, highlighting areas requiring significant improvement in landmark detection.

Table 3 depicts the mAP scores across four landmark categories: Cusp, Facial, Inner/Outer, and Mesial/Distal. This table provides valuable insights into the category-specific performance of the teams. Radboud team (Niels van Nistelrooij *et al.*) and ChohoTech team (Huikai Wu) consistently achieved high mAP scores across all categories, with notable strengths in the Inner/Outer and Mesial/Distal categories, where their scores exceeded 0.78. Conversely, teams like IGIP-LAB team (Weijie Liu *et al.*) and 3DIMLAND team (Tibor Kubík *et al.*) demonstrated lower mAP scores, particularly in the Mesial/Distal category, suggesting challenges in detecting contact points between teeth.

Table 4 provides a detailed view of the mAR scores for the same landmark categories. The highest mAR values were also observed in teams like Radboud team (Niels van Nistelrooij *et al.*) and ChohoTech team (Huikai Wu), with Radboud team excelling in the Inner/Outer category, achieving a score of 0.661, and performing equally well in the Mesial/Distal category with a score of 0.651. The ChohoTech team demonstrated strong recall performance in the Mesial/Distal category, achieving a score of 0.672. Lower-ranked teams like the IGIP-LAB team (Weijie Liu *et al.*) and 3DIMLAND team (Tibor Kubík *et al.*) struggled once again to achieve recall rates comparable to those of higher-performing teams across all landmark categories.

	<b>Team</b>	<b>Rank Score</b>	<b>mAP</b>	<b>mAR</b>
	Radboud team (Niels van Nistelrooij <i>et al.</i> )	0.9172	0.785	0.656
	ChohoTech team (Huikai Wu)	0.8325	0.775	0.634
	YY-LAB team (Kaibo Shi <i>et al.</i> )	0.6224	0.719	0.579
	YN-LAB team (Zhu Xiaoying <i>et al.</i> )	0.3171	0.643	0.527
	IGIP-LAB team (Weijie Liu <i>et al.</i> )	0.1358	0.590	0.466
	3DIMLAND team (Tibor Kubík <i>et al.</i> )	0.0325	0.578	0.438

Table 2: Team rankings with Rank Score, mAP, and mAR.

Team	AP	AP	AP	AP
	cusp	facial	inner_outer	mesial_distal
 Radboud team (Niels van Nistelrooij <i>et al.</i> )	0.772	0.768	0.793	0.792
 ChohoTech team (Huikai Wu)	0.765	0.761	0.780	0.781
 YY-LAB team (Kaibo Shi <i>et al.</i> )	0.684	0.726	0.748	0.705
 YN-LAB team (Zhu Xiaoying <i>et al.</i> )	0.656	0.667	0.610	0.657
 IGIP-LAB team (Weijie Liu <i>et al.</i> )	0.636	0.590	0.634	0.523
 3DIMLAND team (Tibor Kubík <i>et al.</i> )	0.594	0.621	0.551	0.575

Table 3: Detailed mAP Scores by Landmark Category.

Team	AR	AR	AR	AR
	cusp	facial	inner_outer	mesial_distal
 Radboud team (Niels van Nistelrooij <i>et al.</i> )	0.675	0.637	0.661	0.651
 ChohoTech team (Huikai Wu)	0.627	0.586	0.625	0.672
 YY-LAB team (Kaibo Shi <i>et al.</i> )	0.719	0.569	0.601	0.576
 YN-LAB team (Zhu Xiaoying <i>et al.</i> )	0.538	0.522	0.511	0.539
 IGIP-LAB team (Weijie Liu <i>et al.</i> )	0.519	0.445	0.505	0.410
 3DIMLAND team (Tibor Kubík <i>et al.</i> )	0.457	0.459	0.459	0.459

Table 4: Detailed mAR Scores by Landmark Category.

Figures 9 and 10 provide an analysis of the distribution of the values for mAP and mAR metrics across scans and categories, respectively. From the boxplots of mAP and mAR across different categories, it is evident that the Radboud team (Niels van Nistelrooij *et al.*) demonstrates the most consistent performance, with narrow boxes and high median values for both metrics. This consistency shows that their model reliably performs well across various scans, exhibiting stable results. In addition, the ChohoTech team (Huikai Wu) shows a performance very similar to Radboud, with only a high median value in the Mesial/Distal category for the mAR metric.

In contrast, teams such as 3DIMLAND and IGIP-LAB exhibit greater variability in their performance, as indicated by wider boxes. This shows that their models' performance is inconsistent across scans, with some scans yielding high performance and others much lower, showing potential instability or difficulty in handling certain data types or conditions.

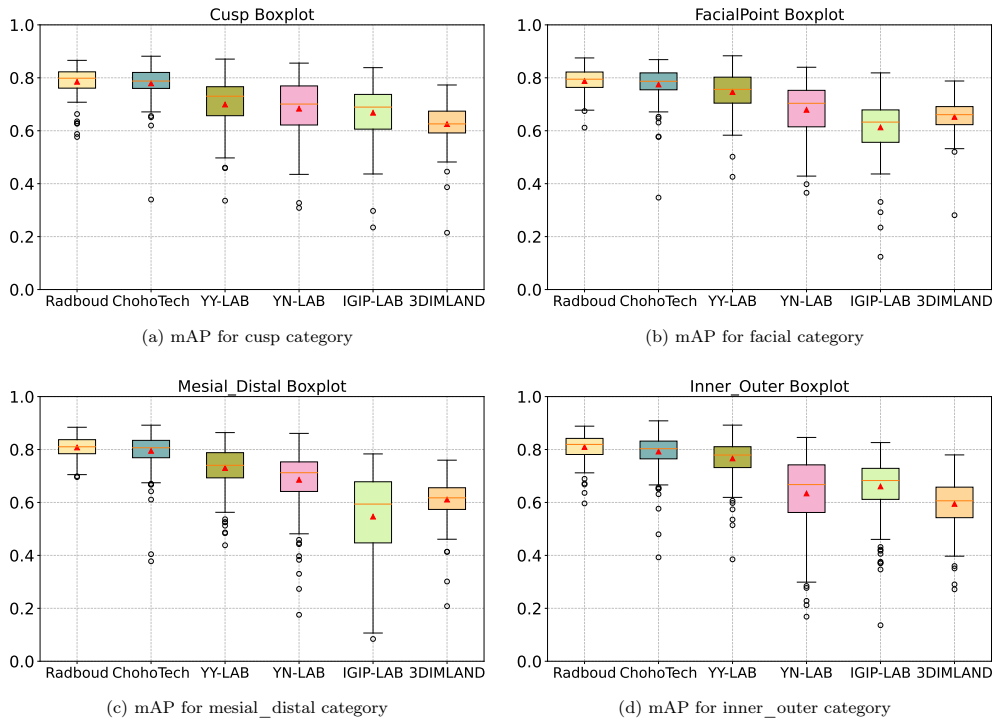


Figure 9: mAP score for each landmark category per scan.

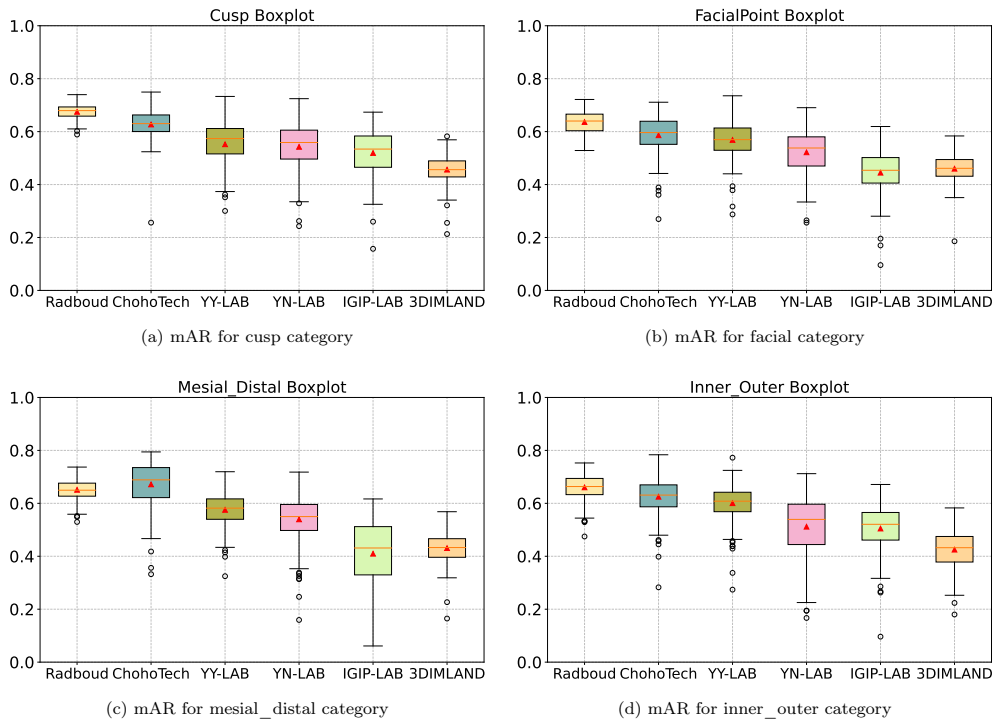


Figure 10: mAR score for each landmark category per scan.

Figure 11 provides an overall visual comparison of landmark detection obtained by the six methods. Each column represents a lower jaw example, allowing for a direct comparison of how well each team’s method performs. Notably, the Radboud team’s approach shows the best alignment between the detected landmarks and the ground truth, indicating a higher level of accuracy and consistency in landmark localization. On the other hand, the 3DIMLAND team’s approach struggles with missing or mislocated landmarks.

Figure 12 presents examples of challenging cases where the proposed methods failed to accurately detect all landmarks. In the final case (fourth column), none of the teams successfully identified all the ground-truth landmarks. The Radboud and YY-LAB teams missed some cusp points, while the Chohotech, YN-LAB, IGIP-LAB, and 3DIMLAND teams failed to detect landmarks on the right half of the jaw. In the second case (second column), the Chohotech and YY-LAB teams misclassified some landmarks, with some distal points labeled as mesial and some mesial points labeled as distal.

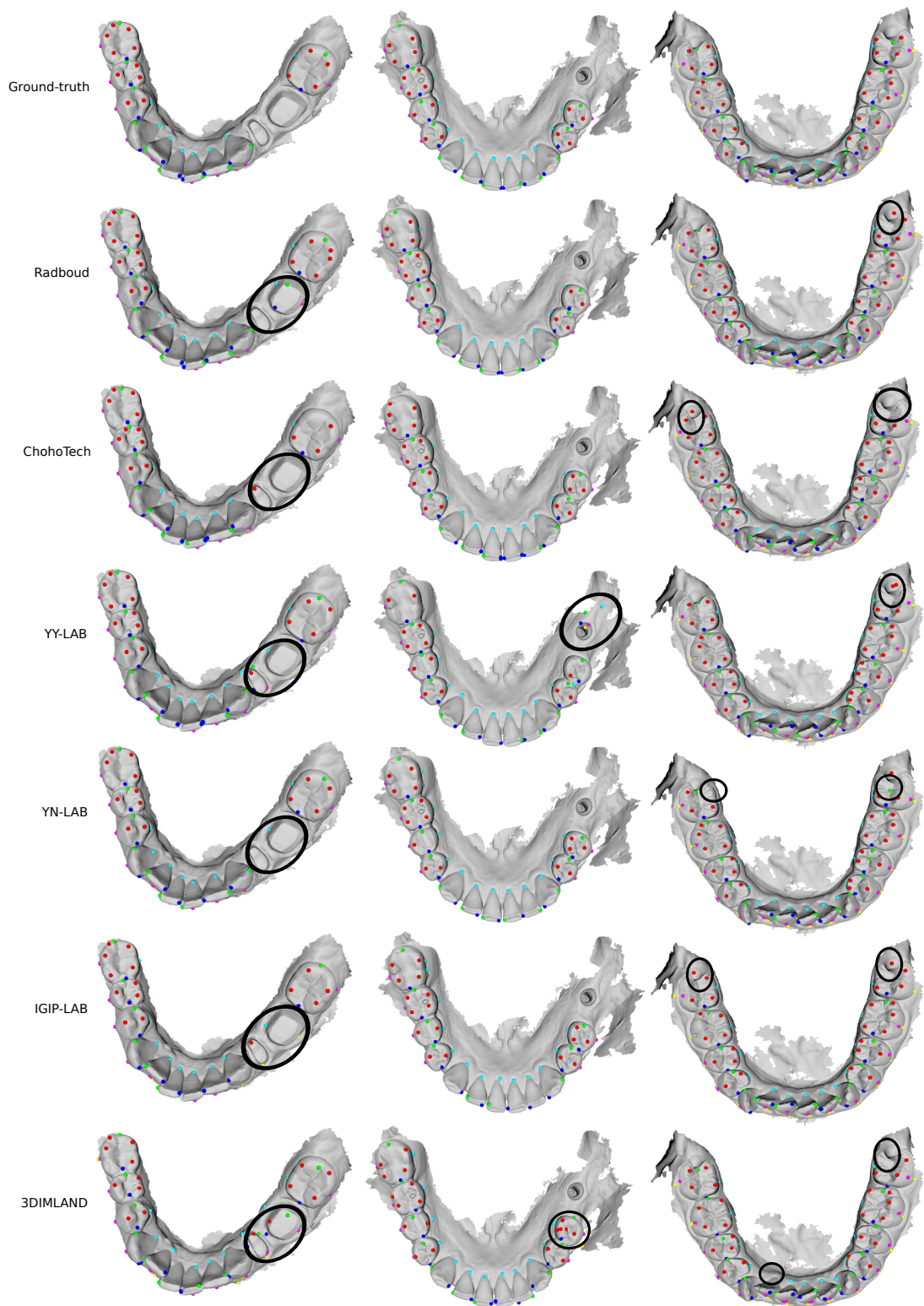


Figure 11: Overall visual comparison of landmark detection obtained by the six methods. Each column corresponds to an example of a lower jaw. Black ellipses denote examples of undetected landmarks or localization errors.

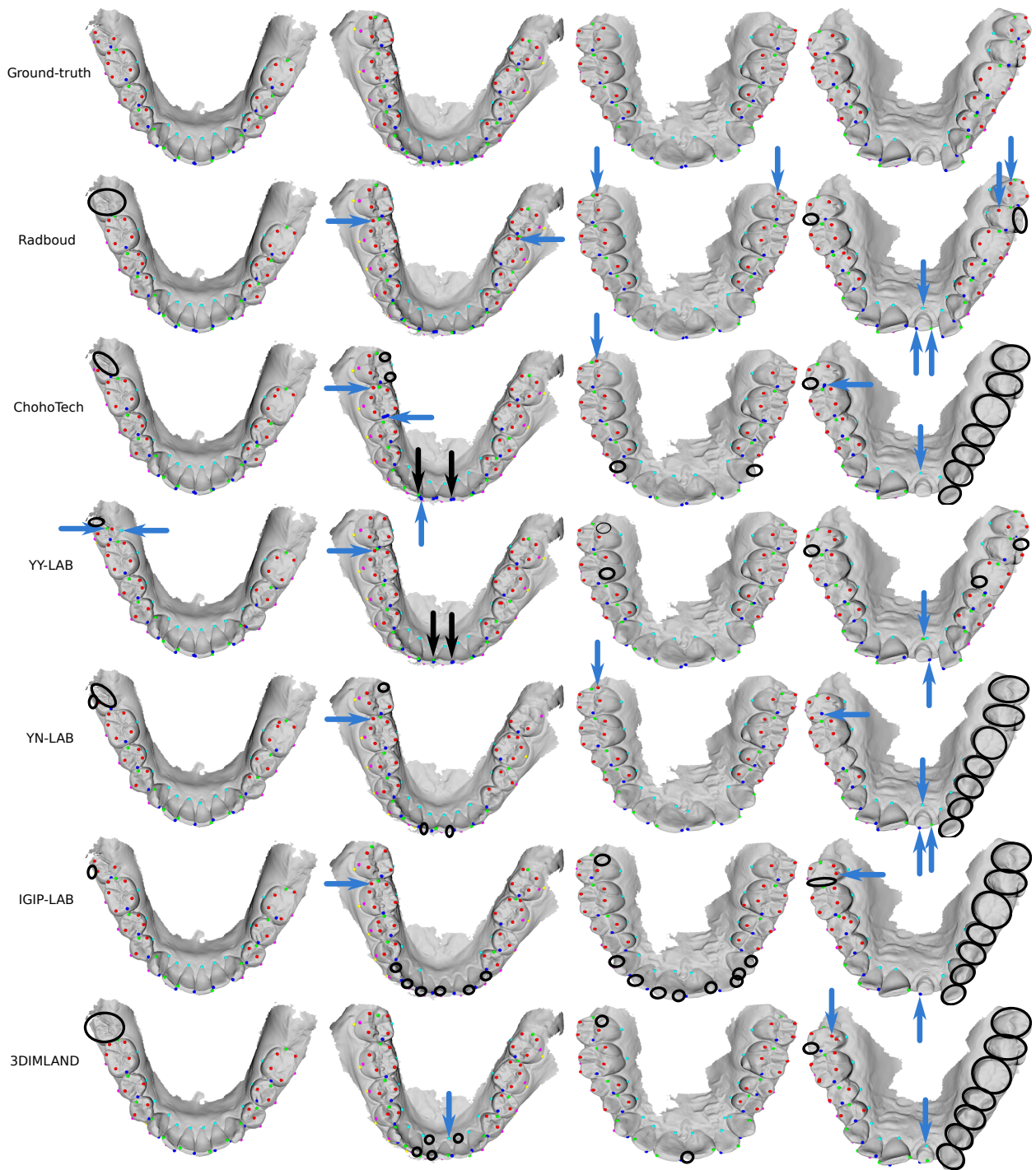


Figure 12: Visual comparison of hard cases for landmark detection obtained by the six methods. The first and second columns correspond to examples of a lower jaw. The third and fourth columns depict examples of an upper jaw. Black ellipses denote examples of undetected landmarks. Examples of errors in landmarks are marked with blue arrows, while category errors are marked with black arrows.

#### 5.4. Discussion

The results from the previous tables and boxplot figures highlight a clear performance gap between the top-performing teams and the lower-ranked ones. The Radboud and ChohoTech teams consistently outperformed others in both precision and recall, showcasing the effectiveness of their approaches in landmark detection. In contrast, teams like IGIP-LAB and 3DIMLAND struggled to achieve comparable results, underscoring areas in their methods that require significant improvement. By examining the methods, we identify three high-level features of the approaches that seem to have relevance to their performance, namely the runtime complexity, the use or absence of segmentation, and the mathematical problem statement (regression vs. classification). We next discuss the observed trends.

**Runtime.** The evaluation of these approaches can be expanded by considering factors such as model complexity, including computational resources, which affect real-world applicability. Additionally, time consumption is crucial for assessing the feasibility of these methods, particularly for large-scale or real-time tasks. Table 5 presents a comparative analysis of the total time taken and the average processing time per scan for different teams. Each team’s approach varies significantly in terms of computational complexity. Although the Radboud team stands out as one of the most effective, their approach has a relatively high total processing time (2125.3 seconds). Conversely, the 3DIMLAND and ChohoTech teams achieved the lowest processing times, with averages of 10.67 and 10.89 seconds per scan, respectively. Notably, the ChohoTech team achieved results comparable to the Radboud team’s best model in terms of mAP and mAR, demonstrating that their approach balances efficiency and accuracy effectively. In contrast, while the 3DIMLAND team achieved the fastest processing time, their performance in mAP and mAR is lower.

**Segmentation.** The six approaches are divided into two categories: those that perform segmentation before landmark detection (*i.e.*, Radboud, YY-LAB, and YN-LAB teams) and those that do not involve tooth segmentation (*i.e.*, ChohoTech, IGIP-LAB, and 3DIMLAND teams). From Table 5, we observe that not involving segmentation leads to a significant reduction in processing time. However, its impact on model performance varies. For instance, the ChohoTech team, which does not use tooth segmentation, achieved the second-best performance while also having one of the lowest processing times. This demonstrates that segmentation may not always be necessary for high accuracy, especially if the model is

Team	Total Time (sec)	Avg/scan (sec)
 Radboud team (Niels van Nistelrooij <i>et al.</i> )	2125.3	21.25
 ChohoTech team (Huikai Wu)	1089.9	10.89
 YY-LAB team (Kaibo Shi <i>et al.</i> )	2289.7	22.89
 YN-LAB team (Zhu Xiaoying <i>et al.</i> )	2962.3	29.62
 IGIP-LAB team (Weijie Liu <i>et al.</i> )	1313.5	13.13
 3DIMLAND team (Tibor Kubík <i>et al.</i> )	1067.5	10.67

Table 5: Time-consuming per team.

well-optimized. On the other side, the IGIP-LAB and 3DIMLAND teams also skipped the segmentation step, resulting in faster processing times but at the cost of reduced performance. This indicates that while removing segmentation improves computational efficiency, its impact on landmark detection accuracy largely depends on the overall effectiveness of the approach.

**Regression vs classification-based approaches.** In the six proposed dental landmark detection approaches, both regression-based and classification-based methods are applied. However, neither of these methods provides direct, precise localization of the landmarks, which necessitates the use of post-processing steps. In regression-based methods, the network typically generates a set of landmark proposals. However, these proposals may be incorrectly placed or located close to each other. To address this, additional steps like filtering and clustering are required. For instance, the Radboud team proposed an interesting filtering technique applied to the predicted distances and offsets. These offsets are used to adjust the coordinates of landmark proposals within a category. Then, a clustering step using the DBSCAN algorithm groups the proposals, and the final position of each landmark is determined by computing the weighted average of the proposals in each cluster. On the other hand, classification-based approaches face the challenge of data imbalance, where the model tends to focus on larger or more common regions. To solve this, various strategies were employed. For example, YN-Lab used curriculum learning, which helps the model gradually handle smaller, more difficult regions, improving its ability to detect landmarks accurately. In this context, the clustering HDBSCAN algorithm is employed to group the points belonging to a specific landmark’s label. After clustering, Gaussian weighted voting is applied to the points within each cluster, where the weighted mean of these points provides a smoother and more accurate estimate of the landmark’s final position. Some other approaches from the six teams combine both classification and regression to leverage the strengths of each approach. For example, the Chohotech team proposed a dual-output network, with one branch predicting a probability heatmap that estimates the likelihood of a point being a landmark, and another branch predicting offsets or residual vectors that refine the initial landmark predictions. This design facilitates more precise adjustments to the landmark positions. As with the other proposed methods, post-processing steps are crucial for improving the accuracy and robustness of the final results. These include threshold filtering, which is applied to the predicted heatmap to filter out points with low confidence, reducing the risk of false positives. In addition, Non-Maximum Suppression (NMS) is used, which eliminates redundant detections and ensures that only the most confident and spatially accurate landmarks are selected.

## 6. Conclusion

The 3DTeethLand challenge, organized in collaboration with the International Conference on Medical Image Computing and Computer-Assisted Intervention (MICCAI) in 2024, focused on the development of algorithms for detecting teeth landmarks from intraoral 3D scans. This challenge marked the introduction of the first publicly available dataset for 3D teeth landmark detection, providing a crucial resource to foster community engagement in

this vital area with considerable clinical implications.

Out of a total of 49 teams that officially participated in the 3DTeethLand challenge, six landmark detection algorithms were evaluated. This paper offers a comprehensive overview of the challenge setup, summarizes the algorithms submitted by the participating teams, and provides a detailed comparison of their performance.

During the final testing phase of the 3DTeethLand challenge, the algorithms were thoroughly evaluated on their ability to accurately detect teeth landmarks across a variety of intraoral 3D scans. The performance of each algorithm was assessed using key metrics, including the mAP and the mAR, which provided insights into both the accuracy and consistency of landmark detection. The top-performing teams consistently achieved high mAP and mAR values, indicating robust precision and recall across different scans and categories. Notably, the Radboud and ChohoTech teams exhibited superior performance. In contrast, other algorithms, such as those from the IGIP-LAB and 3DIMLAND teams, ranked lowest, needing improvement for a more stable and reliable landmark detection across diverse intraoral scans.

As a future direction, enriching the proposed dataset is essential. To further enhance its representativeness of diverse clinical settings, future versions could include a broader range of variations, encompassing a wider demographic spectrum and various dental conditions. Additionally, incorporating more challenging real-world conditions, such as varying levels of noise and incomplete scans, would better prepare algorithms for the complexities encountered in clinical environments. This would contribute to improving the reliability and generalization of landmark detection models.

## Acknowledgements

This work was primarily supported by the Digital Research Center of Sfax, Tunisia.

## Appendix

This section presents additional technical details related to the challenge that are not included in the main text but are essential for a complete and transparent description.

*TimeTable:* Registration opened on the 1st of May, 2024, allowing teams to enroll and prepare for participation. The first batch of training data was released on the 27th of May, 2024, followed by the second batch on the 15th of June, 2024, enabling participants to begin data exploration and model development. The public test set became available on the 30th of July, 2024, at which time the submission portal for public test evaluation also opened. The Final Phase began on the 26th of September, 2024, with the opening of the evaluation pipeline for final submissions. Teams were required to upload their Docker containers by the submission deadline on the 2nd of October, 2024. Algorithm descriptions and related papers were shared on the 29th of September, 2024, as part of the challenge documentation process. The challenge concluded on the 6th of October, 2024, during the MICCAI 2024 event.

*Organization:* 3DTeethLand is the successor to the 3DTeethSeg challenge, held as a recurring annual event with a fixed submission deadline. All evaluated algorithms are required to operate in a fully automatic manner, without any user interaction.

*Publication.* Throughout the challenge, participants had access to the GitHub repository <sup>5</sup>, where they could find the source code for the evaluation script as well as a Docker template containing a baseline algorithm to be replaced for participation. All teams were required to share their code with the organizers for evaluation, and this step was mandatory for the top-ranking methods.

Each member of the team is listed as an author for the corresponding submission. This paper provides an overview of the challenge results and key proposals, including all contributors as co-authors. Participants are allowed to publish their own results independently after an embargo time of 6 months after the MICCAI event.

*Author contributions:* **Conceptualization:** Achraf Ben-Hamadou, Nour Neifar, Ahmed Rekik, Oussama Smaoui, Firas Bouzguenda, Sergi Pujades. **Methodology:** Achraf Ben-Hamadou, Nour Neifar, Ahmed Rekik, Oussama Smaoui, Firas Bouzguenda, Sergi Pujades. **Evaluation Script:** Oussama Smaoui. **Software challenge Submission:** Niels van Nistelrooij, Shankeeth Vinayahalingam, Kaibo Shi, Hairong Jin, Youyi Zheng, Tibor Kubík, Oldřich Kodým, Petr Šilling, Kateřina Trávníčková, Tomáš Mojžíš, Jan Matula, Xiaoying Zhu, Jeffry Hartanto, Kim-Ngan Nguyen, Tudor Dascalu, Huikai Wu, Weijie Liu, Shaojie Zhuang, Guangshun Wei, Yuanfeng Zhou. **Validation:** Achraf Ben-Hamadou, Nour Neifar, Ahmed Rekik, Oussama Smaoui. **Writing, Review and Editing:** Achraf Ben-Hamadou, Nour Neifar, Ahmed Rekik, Oussama Smaoui, Sergi Pujades.

*Conflicts of interest:* There are no conflicts of interest. Udini is the principal sponsor of the challenge by collecting and providing clinical data with the contribution of the Digital Research Center of Sfax. Only the organizers and members of their immediate team have access to test case labels.

## References

- [1] F. Angelone, A. M. Ponsiglione, C. Ricciardi, G. Cesarelli, M. Sansone, F. Amato, Diagnostic Applications of Intraoral Scanners: A Systematic Review, *Journal of Imaging* 9 (7) (2023) 134.
- [2] S. Logozzo, E. M. Zanetti, G. Franceschini, A. Kilpelä, A. Mäkynen, Recent advances in dental optics – Part I: 3D intraoral scanners for restorative dentistry, *Optics and lasers in engineering* 54 (2014) 203–221.
- [3] F. Eggmann, M. Blatz, Recent Advances in Intraoral Scanners, *Journal of Dental Research* 103 (13) (2024) 1349–1357.
- [4] B. Woodsend, E. Koufoudaki, P. A. Mossey, P. Lin, Automatic recognition of landmarks on digital dental models, *Computers in Biology and Medicine* 137 (2021) 104819.

---

<sup>5</sup><https://github.com/crns-smartvision/3DTeethLand/tree/master>

- [5] M. Palone, G. A. Spedicato, L. Lombardo, Analysis of tooth anatomy in adults with ideal occlusion: A preliminary study, *American Journal of Orthodontics and Dentofacial Orthopedics* 157 (2) (2020) 218–227.
- [6] F. Bolelli, L. Lumetti, S. Vinayahalingam, M. Di Bartolomeo, A. Pellacani, K. Marchesini, N. Van Nistelrooij, P. Van Lierop, T. Xi, Y. Liu, et al., Segmenting the Inferior Alveolar Canal in CBCTs Volumes: The ToothFairy Challenge, *IEEE Transactions on Medical Imaging* (2024).
- [7] Y. Wang, Y. Zhang, X. Chen, S. Wang, D. Qian, F. Ye, F. Xu, H. Zhang, R. Dan, Q. Zhang, et al., MICCAI 2023 STS Challenge: A retrospective study of semi-supervised approaches for teeth segmentation, *Pattern Recognition* (2025) 112049.
- [8] A. Ben-Hamadou, O. Smaoui, A. Rekik, S. Pujades, E. Boyer, H. Lim, M. Kim, M. Lee, M. Chung, Y.-G. Shin, et al., 3DTeethSeg’22: 3D Teeth Scan Segmentation and Labeling Challenge, *arXiv preprint arXiv:2305.18277* (2023).
- [9] A. Rekik, A. Ben-Hamadou, O. Smaoui, F. Bouzguenda, S. Pujades, E. Boyer, TSegLab: Multi-stage 3D dental scan segmentation and labeling, *Computers in Biology and Medicine* 185 (2025) 109535.
- [10] S. Triarjo, R. Sarno, S. C. Hidayati, G. Sihaj, Automatic 3D Digital Dental Landmark Based on Point Transformation Weight , in: *2023 International Conference on Artificial Intelligence in Information and Communication (ICAIIIC)*, IEEE, 2023, pp. 336–341.
- [11] T.-H. Wu, C. Lian, S. Lee, M. Pastewait, C. Piers, J. Liu, F. Wang, L. Wang, C.-Y. Chiu, W. Wang, et al., Two-Stage Mesh Deep Learning for Automated Tooth Segmentation and Landmark Localization on 3D Intraoral Scans , *IEEE transactions on medical imaging* 41 (11) (2022) 3158–3166.
- [12] G. Wei, Z. Cui, J. Zhu, L. Yang, Y. Zhou, P. Singh, M. Gu, W. Wang, Dense Representative Tooth Landmark/axis Detection Network on 3D Model , *Computer Aided Geometric Design* 94 (2022) 102077.
- [13] Y. Lang, X. Chen, H. H. Deng, T. Kuang, J. C. Barber, J. Gateno, P.-T. Yap, J. J. Xia, DentalPointNet: landmark localization on high-resolution 3D digital dental models, in: *International Conference on Medical Image Computing and Computer-Assisted Intervention*, Springer, 2022, pp. 444–452.
- [14] Y. Lang, H. H. Deng, D. Xiao, C. Lian, T. Kuang, J. Gateno, P.-T. Yap, J. J. Xia, DLLNet: An Attention-Based Deep Learning Method for Dental Landmark Localization on High-Resolution 3D Digital Dental Models, in: *Medical Image Computing and Computer Assisted Intervention–MICCAI 2021: 24th International Conference, Strasbourg, France, September 27–October 1, 2021, Proceedings, Part IV 24*, Springer, 2021, pp. 478–487.

- [15] T. Kubík, M. Španěl, Robust Teeth Detection in 3D Dental Scans by Automated Multi-View Landmarking, in: Proceedings of the 15th International Joint Conference on Biomedical Engineering Systems and Technologies - BIOIMAGING, SciTePress, 2022, pp. 24–34.
- [16] C. Lian, L. Wang, T.-H. Wu, F. Wang, P.-T. Yap, C.-C. Ko, D. Shen, Deep Multi-Scale Mesh Feature Learning for Automated Labeling of Raw Dental Surfaces From 3D Intraoral Scanners , IEEE transactions on medical imaging 39 (7) (2020) 2440–2450.
- [17] C. Lian, L. Wang, T.-H. Wu, M. Liu, F. Durán, C.-C. Ko, D. Shen, MeshSNet: Deep Multi-scale Mesh Feature Learning for End-to-End Tooth Labeling on 3D Dental Surfaces, in: Medical Image Computing and Computer Assisted Intervention – MICCAI 2019, Springer, 2019, pp. 837–845.
- [18] A. Ben-Hamadou, N. Neifar, A. Rekik, O. Smaoui, F. Bouzguenda, S. Pujades, E. Boyer, E. Ladroit, Teeth3DS+: An Extended Benchmark for Intraoral 3D Scans Analysis , arXiv preprint arXiv:2210.06094 (2022).
- [19] M. Ester, H.-P. Kriegel, J. Sander, X. Xu, A density-based algorithm for discovering clusters in large spatial databases with noise, in: Proceedings of the Second International Conference on Knowledge Discovery and Data Mining, AAAI Press, 1996, p. 226–231.
- [20] M. Garland, P. S. Heckbert, Surface Simplification Using Quadric Error Metrics, in: Proceedings of the 24th annual conference on Computer graphics and interactive techniques, ACM Press/Addison-Wesley Publishing Co., 1997, pp. 209–216.
- [21] Y. Zheng, B. Chen, Y. Shen, K. Shen, TeethGNN: Semantic 3D Teeth Segmentation With Graph Neural Networks, IEEE Transactions on Visualization and Computer Graphics 29 (7) (2022) 3158–3168.
- [22] H. Jin, Y. Shen, J. Lou, K. Zhou, Y. Zheng, KeypointDETR: An End-to-End 3D Keypoint Detector, in: European Conference on Computer Vision, Springer, 2025, pp. 374–390.
- [23] Y. Bengio, J. Louradour, R. Collobert, J. Weston, Curriculum learning, in: Proceedings of the 26th annual international conference on machine learning, 2009, pp. 41–48.
- [24] T. Dascalu, B. Ibragimov, Assignment Theory-Augmented Neural Network for Dental Arch Labeling, in: International Conference on Medical Image Computing and Computer-Assisted Intervention, Springer, 2023, pp. 295–304.
- [25] J. Li, J. Zhou, Y. Xiong, X. Chen, C. Chakrabarti, An Adjustable Farthest Point Sampling Method for Approximately-sorted Point Cloud Data, in: 2022 IEEE Workshop on Signal Processing Systems (SiPS), IEEE, 2022, pp. 1–6.

- [26] X. Ma, C. Qin, H. You, H. Ran, Y. Fu, Rethinking network design and local geometry in point cloud: A simple residual MLP framework, arXiv preprint arXiv:2202.07123 (2022).
- [27] T.-H. Tran, T.-D. Cao, T.-T.-H. Tran, HDBSCAN: Evaluating the Performance of Hierarchical Clustering for Big Data, in: *Soft Computing: Biomedical and Related Applications*, Springer, 2021, pp. 273–283.
- [28] Y. You, et al., KeypointNet: A Large-scale 3D Keypoint Dataset Aggregated from Numerous Human Annotations , in: *2020 IEEE/CVF Conference on Computer Vision and Pattern Recognition (CVPR)*, IEEE, 2020, pp. 13644–13653.
- [29] L. Maier-Hein, A. Reinke, P. Godau, M. D. Tizabi, F. Buettner, E. Christodoulou, B. Glocker, F. Isensee, J. Kleesiek, M. Kozubek, et al., Metrics reloaded: Recommendations for image analysis validation , *Nature methods* 21 (2) (2024) 195–212.